



OPEN ACCESS

EDITED BY
Candan Gokceoglu,
Hacettepe University, Turkey

REVIEWED BY
Mohammad Reza Zareifard,
Estahban Higher education center, Iran
Chong Xu,
Ministry of Emergency Management,
China

*CORRESPONDENCE
Jian Zhang,
jianzhang_1018@126.com

SPECIALTY SECTION
This article was submitted to
Geohazards and Georisks,
a section of the journal
Frontiers in Earth Science

RECEIVED 20 July 2022
ACCEPTED 30 August 2022
PUBLISHED 28 September 2022

CITATION
Zhang J, Cao L and Shen H (2022),
Typical site seismic response analysis
with reinforcement under earthquake
and rainfall in the mountainous areas
of China.
Front. Earth Sci. 10:998745.
doi: 10.3389/feart.2022.998745

COPYRIGHT
© 2022 Zhang, Cao and Shen. This is an
open-access article distributed under
the terms of the [Creative Commons
Attribution License \(CC BY\)](https://creativecommons.org/licenses/by/4.0/). The use,
distribution or reproduction in other
forums is permitted, provided the
original author(s) and the copyright
owner(s) are credited and that the
original publication in this journal is
cited, in accordance with accepted
academic practice. No use, distribution
or reproduction is permitted which does
not comply with these terms.

Typical site seismic response analysis with reinforcement under earthquake and rainfall in the mountainous areas of China

Jian Zhang^{1*}, Licong Cao² and Hao Shen²

¹School of Design, Southwest Jiaotong University, Chengdu, China, ²School of Architecture, Southwest Jiaotong University, Chengdu, China

Multi-tilted layered soil is widespread in the mountainous areas of China, and pile systems are widely applied to foundation support and repair. In order to investigate the seismic response of pile systems in multi-tilted layered soils under earthquake and rainfall, two models were built and tested through a large 1-g shaking table. The interlayer was tilted and highly weathered, and it was saturated during rainfall. The piles were embedded in the bedrock with different lengths. The results showed that: 1) The acceleration response was weakened in the interlayer, and it diminished as the earthquake amplitude increased. The structures showed the maximum acceleration response. 2) The existence of water in the tilted interlayer led to a greater response of the superstructure. The bending moment of piles varied under different containers, which was mainly due to the inertial force of the container and the potential sliding force of the covering layer. The water in the interlayer from rainfall promoted the bending moment caused by the potential sliding force, increasing the potential risk of instability of the system. 3) The motion mode of the container under rainfall was translation. The rotation angle of the container with saturated moisture content was significant and it increased with the increase of the earthquake amplitude.

KEYWORDS

rainfall, earthquake, seismic response, multi-tilted-layered soil, bending moment

Introduction

Multi-tilted layered soil is widespread in the mountainous areas of China. Seismic data indicates that the proportion of land area with high-intensity earthquake potential in China where the intensity degree is greater than VII is more than 50% based on the “Chinese Seismic Intensity Scale” (GB/T 17742-2008, 2008). Landslides provoked by earthquakes are common in this region. Besides, rainfall should not be ignored when performing site stability evaluations, as the subsequent rainfalls increased landslides by 68% in the Wenchuan earthquake-hit area (Tang et al., 2010).

Some researchers studied landslide susceptibility assessments using mathematical models (Jiang and Huang, 2016; Guo et al., 2021; Huang et al., 2021). Pile systems were widely applied to foundation support and repair of soil in potential landslide risk area, and their performance under

static and dynamic loadings was studied by researchers. Earthquake loading is considered to play a significant role in designing the pile foundation and studying the dynamic response (Tokimatsu et al., 2005; Maiorano et al., 2009; Badry and Satyam, 2017).

Meanwhile, multi-layered soil with different stiffness is common, and it is important to build pile-supported structures whose piles are in this type of soil. The pile may be damaged during an earthquake, and the failure mode is significantly determined by the pile stiffness (Martin and Chen, 2005). Furthermore, rainfall should not be ignored because it is often accompanied by earthquakes and aftershocks. For example, rainfall happened frequently during the Wenchuan earthquake aftershock period, and more landslides were triggered by the coupled condition of aftershocks and rainfall (Tang et al., 2010). Researchers focused on physical models and mathematical statics models to study the rainfall-induced landslide. Ciurleo et al. (2018) and Michel et al. (2014) conducted physical experiments to explore the threshold of critical rainfall that created the slope instability. Adler (2008), Segoni et al. (2018) and Huang et al. (2021, 2022a, 2022b) researched the landslide early warning under rainfall. Samuele et al. (2018) propose a methodology to couple rainfall thresholds and susceptibility maps for dynamic landslide hazard assessment at regional scale. The soil shear strength may be weakened due to the pore-water pressure increase under rainfall (White and Singham, 2012). So, it matters greatly to study the seismic response of nonlinear soil-pile systems in multi-layered soil under earthquakes and rainfall.

More attention has been paid to the soil seismic response or pile dynamic response buried in homogeneous soil or two-layer soil. Wilson (1998) studied the dynamic features of a pile foundation in liquefying sand through centrifuge tests. He et al. (2009) explored the response of single piles embedded in saturated medium relative density sand due to liquefaction-induced lateral soil flow. Tang and Ling (2014) conducted shaking table tests on reinforced concrete cap pile foundations in two-layer soil during soil liquefaction and found that the bending moment of the pile was related to the frequency and amplitude of the earthquake. Mashhoud et al. (2018) explored the dynamic feature of micropiles in loose sand using shaking tables. Liu et al. (2022) investigated the dynamic characteristics of sandy soils with recycled tire rubber. Some numerical simulations were also conducted on this topic (Uzuoka et al., 2007; Elgamel et al., 2008; Choobbasti et al., 2012; Liu et al., 2016; Zhang et al., 2018).

Unlike popular research in the dynamic response of piles in double-layer soil, fewer studies have studied the dynamic response of piles in three-layer soil. Martin and Chen (2005) proposed a displacement method using FLAC 3D software to evaluate the response of piles in three-layer soils to lateral slope movement and found that the relative stiffness between the pile and soil had a great influence on the pile's failure modes. Eight dynamic model tests were performed by Brandenburg et al. (2005) to study the behavior of single piles and pile groups in liquefiable and laterally spreading ground through centrifuge tests; the results reveal that the

liquefaction of the sand layer beneath the crust led to a much larger displacement of the pile cap than expected. Chang and Hutchinson (2013) built a single pile system with no superstructure mass, embedded it in a three-layer soil with 2° of inclination, and mounted it on a shaking table. The pile bottom was fastened to the soil container, and the interlayer was saturated with loose sand. The calculation results show that 1.5D was the pile's plastic region, larger than the assumed value in column capacity design. However, pile groups in tilted multi-layered soils were not considered, and there is no comparison on the responses of models with different moisture content.

Hence, this study took the coupled effects of earthquake and rainfall into consideration for a nonlinear soil-pile system in multi-tilted layered soils. A large 1-g shaking table test was conducted on two different water content models. There were five superstructures on the pile group, and the piles were lined up in a 2×2 manner in each model and were embedded in the bedrock with different lengths. Scaled El Centro earthquakes with different acceleration amplitudes were loaded. The acceleration response, bending moment of the piles, and displacement distribution of superstructure were presented.

Materials and methods

Overview of typical sites

The area we studied is located in the southwestern part of China, as shown in Figure 1. It also shows the epicenter distribution of earthquakes ($M \geq 4.7$) between 186 BC and August 2008 in the Longmenshan fault zone, Sichuan Province. Given the high frequency of earthquakes, superstructures in this region are in great danger. The abundant underground water coming from rainfall also threatens site stability. The geological survey shows that the horizontal angle of tilted interlayer is 17°.

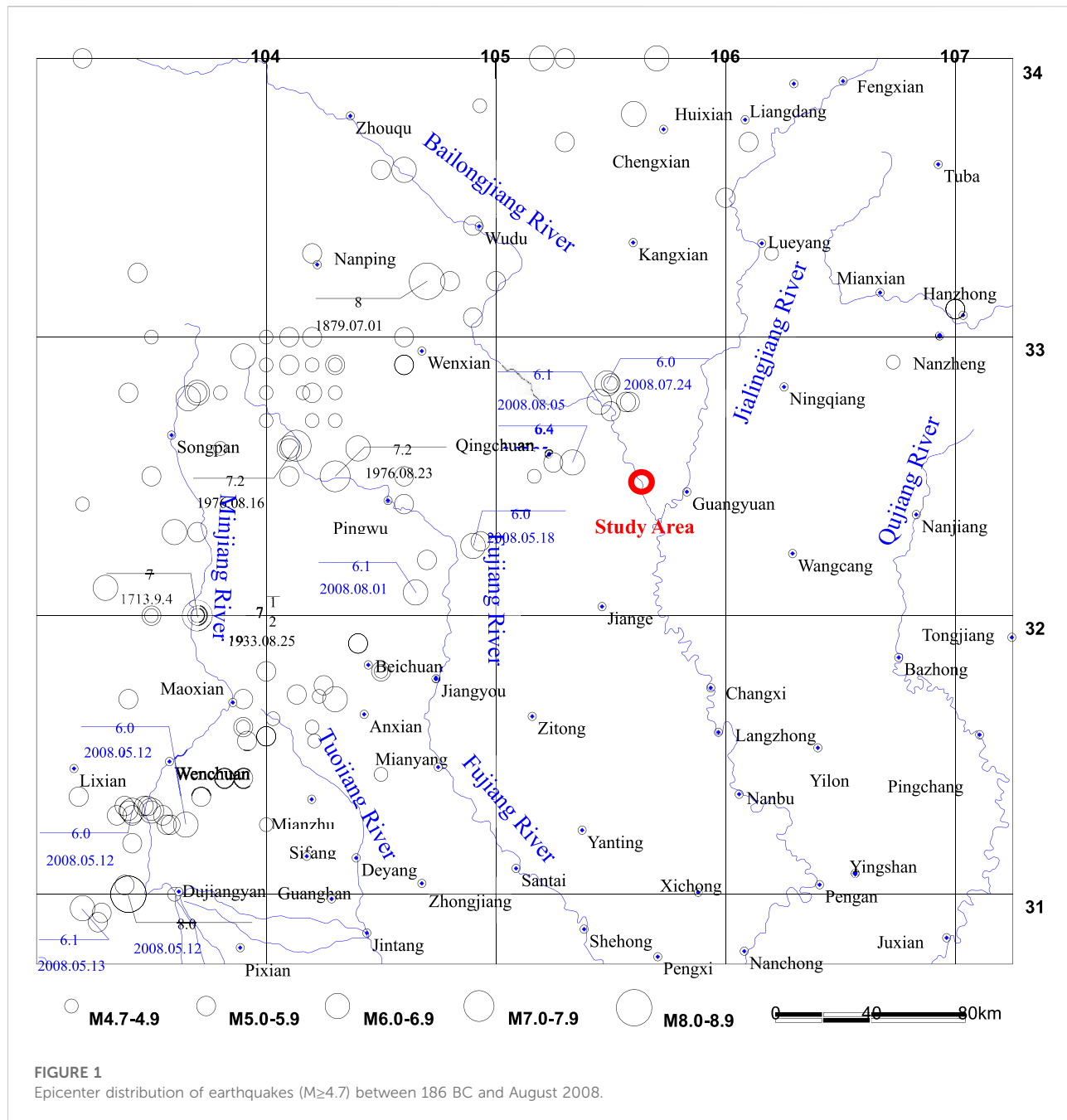
Similitude rules

As shown in Table 1, 17 parameters were chosen as the scale factors for the model test. The gravity acceleration (g) was 1 for the 1-g shaking table test, and other control parameters were geometric dimension (L), density (ρ), and strain (ϵ). The scale factor of dimension λ was 70 according to the prototype and shaking table size. Based on the π theorem by Brand (1957) and experiment design by Curtis et al. (1982) and Meymand (1998), the scale factors of other parameters could be deduced.

Model test

Steel boxes for the model

Figure 2 shows the rigid boxes which were bolted to the platform of shaking table. The containers were 3.5 m (length) ×



1.5 m (width) × 2.5 m (height). Thick foam was used between the soil and box to weaken the boundary effect according to [Bhattacharya et al. \(2012\)](#) and [Cao et al. \(2018\)](#).

Model disposal container

The prototype, a nuclear disposal container, was 52 m (length) × 26 m (width) × 28 m (height) and weighs 17,576 tons. There were 5 containers (1#-5#), and the model container was 750 mm × 175 mm × 400 mm (long × wide × high) and weighed 102.5 kg based on the prototype data and scale factor. The pile cap was

selected as a steel plate, and the thickness was 10 mm. Steel rings were welded with the cap, and the pile and cap were fixed and connected by bolts to simulate rigid connection. Also, rubber was filled in the interspace between the pile and steel ring. The connection simulation was simplified, and it was suitable because this part was safe in model design.

Model piles

The model piles were designed based on the total flexural rigidity similarity of piles (EI similarity). Prototype piles were in

TABLE 1 Scale factors of the soil-pile system model.

Parameters	Scale Factors	Parameters	Scale Factors
Physical dimension/ <i>L</i>	λ	Shear wave velocity/ <i>V_s</i>	$\lambda^{1/2}$
Density/ ρ	1	Time/ <i>T_d</i>	$\lambda^{1/2}$
Gravitational acceleration/ <i>g</i>	1	Inputting acceleration/ <i>A</i>	1
Strain/ ϵ	λ	Frequency/ ω	$\lambda^{-1/2}$
Elasticity modulus/ <i>E</i>	λ	Displacement/ <i>s</i>	λ
Poisson ratio/ μ	1	Velocity/ <i>V</i>	$\lambda^{1/2}$
Cohesion/ <i>C</i>	λ	Angular displacement/ θ	1
Internal friction angle/ Φ	1	Stress/ σ	λ
Outputting acceleration/ <i>a</i>	1		

a group, and the total EI of piles was $8.07e^{24}$ Nmm². The EI of model piles was $4.8e^{15}$ Nmm² based on the flexural rigidity similarity. PVC piles whose outer diameter was 75 mm and thickness was 2.3 mm were suitable in view of the material parameters. Model PVC piles are shown in Figure 3. Four model piles were deployed at the corners of the container. The elasticity modulus of the pile was $3.5e^9$ N•mm². The prototype pile was embedded in the bedrock with at least 1D pile diameter. Table 2 lists the lengths of model piles and shows that the pile lengths were different because of the tilted highly weathered layer.

Model soil layers

The models were built from bottom to top. The angle of the interlayer was set 17° to the horizontal according to the prototype. Wang et al. (2013) in our team proposed the soil design for the simulation test based on *G/G_{max}-γ* curve (*G*: shear modulus; γ : shear stain). The detailed process and material parameter were described in another paper of the same model (but without structure) (Cao et al., 2019).

Test facilities

The study was performed in the Nuclear Power Institute of China which is equipped with a 6 m-wide and 6 m-long shaking table. The parameters are listed in Table 3. Data was collected using a 128-channel data acquisition system.

Test model and deployment of the measured points

The pile group was lined up in 2×2 configuration under each disposal container that weighed 102.5 kg and was fixed on the top

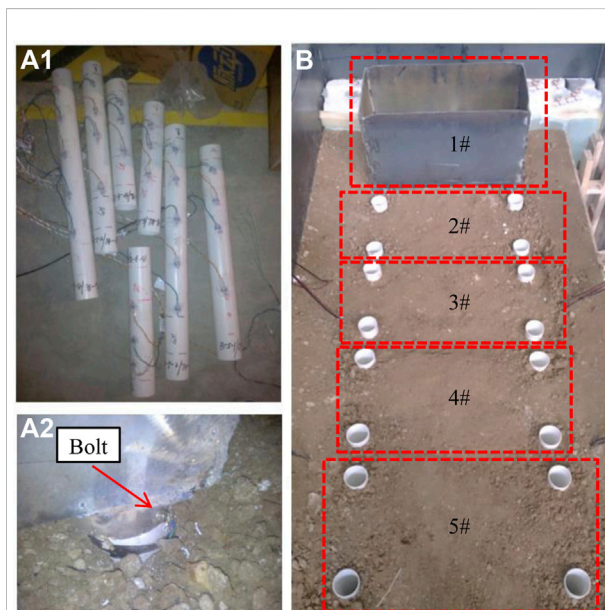


FIGURE 3 Model piles used in the test: (A1) different piles; (A2) details of connection between containers and piles; (B) layout of piles.

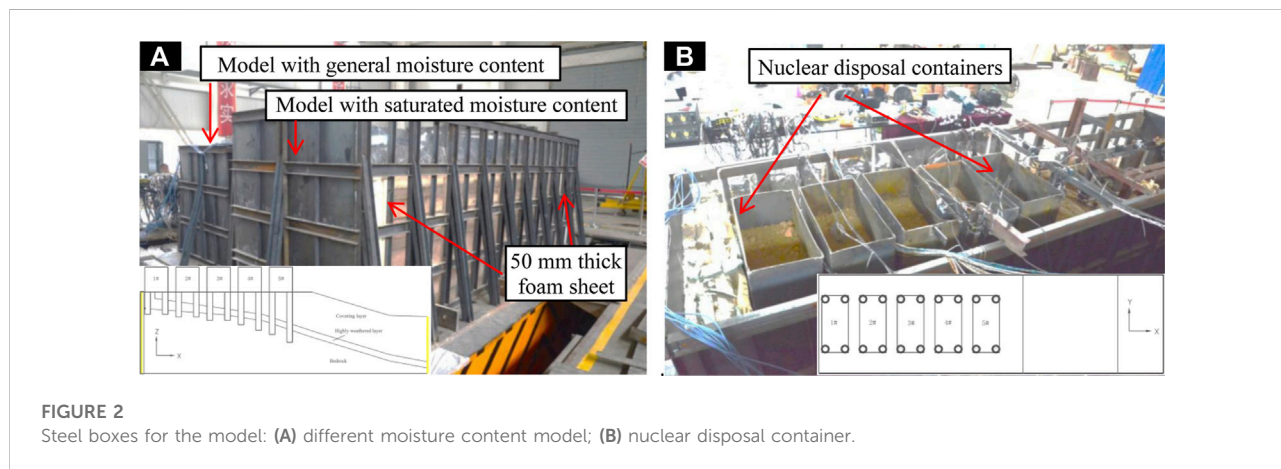


FIGURE 2 Steel boxes for the model: (A) different moisture content model; (B) nuclear disposal container.

TABLE 2 Length of the model piles.

Location	Length (mm)	Location	Length (mm)
1# - P1/P2/P3/P4	350	4# - P2/P4	608
2# - P1/P2/P3/P4	394	5# - P1/P3	660
3# - P1/P2/P3/P4	450	5# - P2/P4	800
4# - P1/P3	520		

of the pile caps. Different sensors were employed to record the whole shaking process, as shown in Figure 4. Ten accelerometers in 3 soil layers, 8 laser displacement transducers on the structures and slope surface, and strain gauges were used in each model. In view of the general features of pile response, the most vulnerable container, and the limit of the number of channels, the piles of containers 3# and 5# were attached with strain gauges as shown in Figure 5. Also, the water content of the interlayer bottom was measured through a soil moisture sensor.

Seismic input motions

The El Centro seismic wave with amplitudes being 0.15, 0.33, 0.5, and 0.7 g and Gaussian stationary white noise (0.1 g) were chosen as excitation. The time was also compressed by 8.37 time based on the scale factor. Figure 6 shows the time history and Fourier spectrum of excited El Centro waves.

Results

It was expected that earthquake wave propagation would be affected when it transmitted in multi-tilted-layered soils. Also, the different water content of the interlayer would influence the acceleration distribution in the soil body. The acceleration response, bending moment response, and displacement response are shown below.

Acceleration response of the system

Twenty accelerometers were used in the 2 models. Acceleration history, Fourier spectrums, and acceleration

amplitude factor were analyzed to study the seismic response of the pile-soil system.

Acceleration history and Fourier spectrums

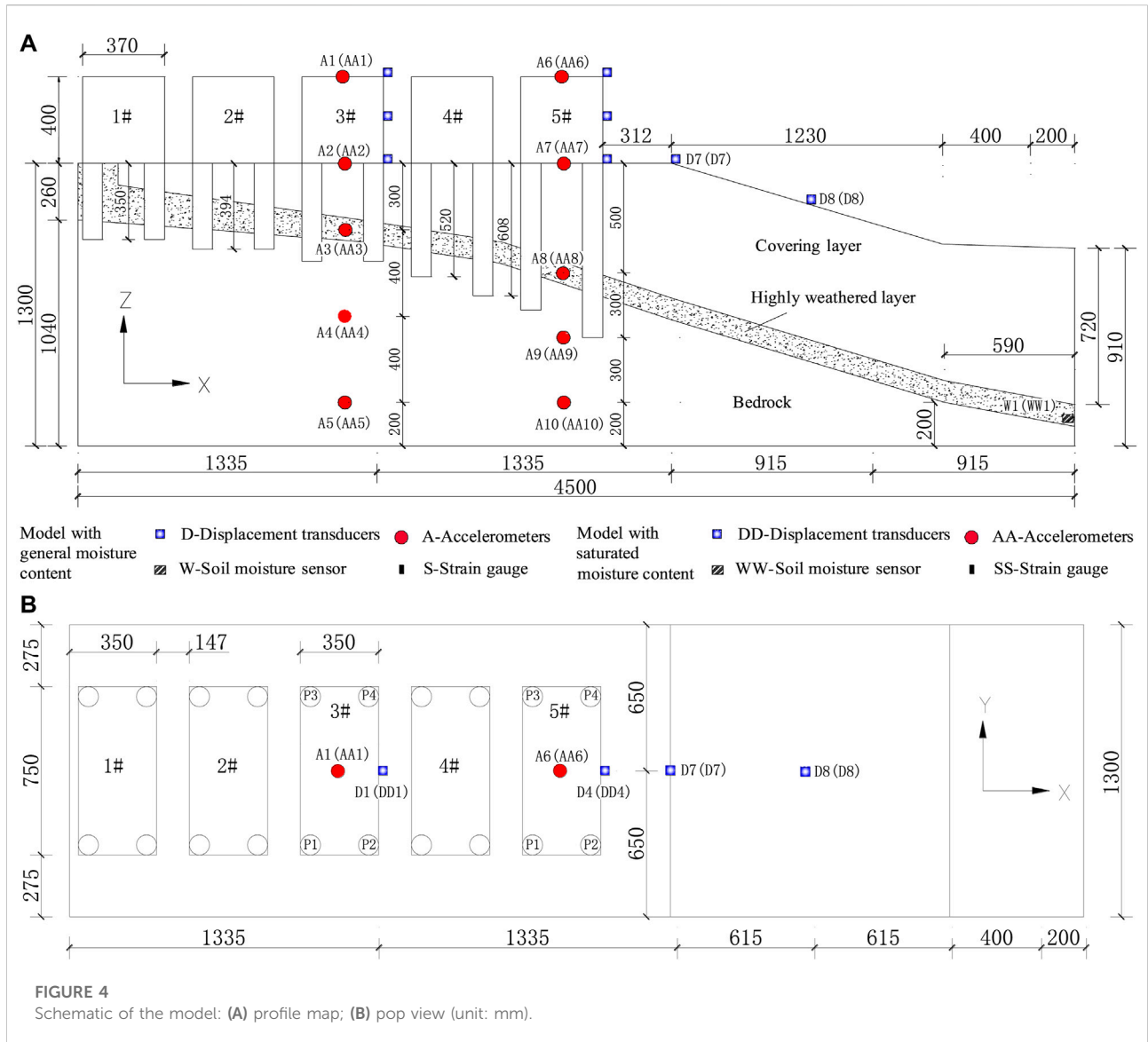
Figure 7 indicates the acceleration time history and the Fourier spectrum of the measured point near container 5# (section II') when the soil was saturated under 0.15 g El Centro earthquake excitation. It shows that the acceleration in the interlayer (AA8) had a deduction of 10.8% compared with the acceleration of point AA9 in the bedrock, then the acceleration became greater in the covering layer and superstructure. The acceleration amplitude of point AA6 on the container was 0.578 g which was 23.5% larger than that of AA7. The Fourier spectrums are also shown in Figure 7; it can be seen that there was an infiltration effect for the weak interlayer with the deduction of Fourier amplitude when the wave propagated upward. The amplitude of the Fourier spectrum for the bedrock was magnified near the frequency 31 Hz compared with that of the loaded wave. Meanwhile, at the frequency near 17 Hz, the amplitude was enhanced in the covering layer and superstructure. The Fourier analysis shows the infiltration of the interlayer and magnification of the covering layer and superstructure.

Acceleration amplitude factor

The acceleration responses of the measured points under wave excitations with different amplitudes were investigated using the acceleration amplitude factor (AAF) which was defined as $AAF = \max [Y_i(t)] / \max [X(t)]$ ($Y_i(t)$: acceleration of the measured point; $X(t)$: bottom acceleration). The AAF distributions near container 3# (section I and section I') and container 5# (section II and section II') are shown in Figure 8 and Figure 9 for both models. It can be seen that the acceleration was nonlinear, especially in the interlayer. The AAF value went up with the elevation of the bedrock and decreased at the interlayer and then rose again in the cover layer before reaching the maximum on the container top. As the interlayer was of low stiffness and low effective stress, more energy would be dissipated, and thus the decrease of AAF occurred. Also, it is shown that the acceleration went down when the earthquake amplitude increased.

TABLE 3 Details of the shaking table.

No.	Parameters	Value	No.	Parameters	Value
1	Freedom Degrees	6	6	Maximum Horizontal Acceleration with Full Load	1g
2	Dimension	6mX6m	7	Maximum Vertical Acceleration with Full Load	0.8g
3	Load Capacity	600KN	8	Maximum Horizontal Acceleration without Load	3g
4	Maximum Horizontal Displacement	±150 mm	9	Maximum Vertical Acceleration without Load	2.6g
5	Maximum Vertical Displacement	±100 mm	10	Output Frequency Range	0.1-80Hz

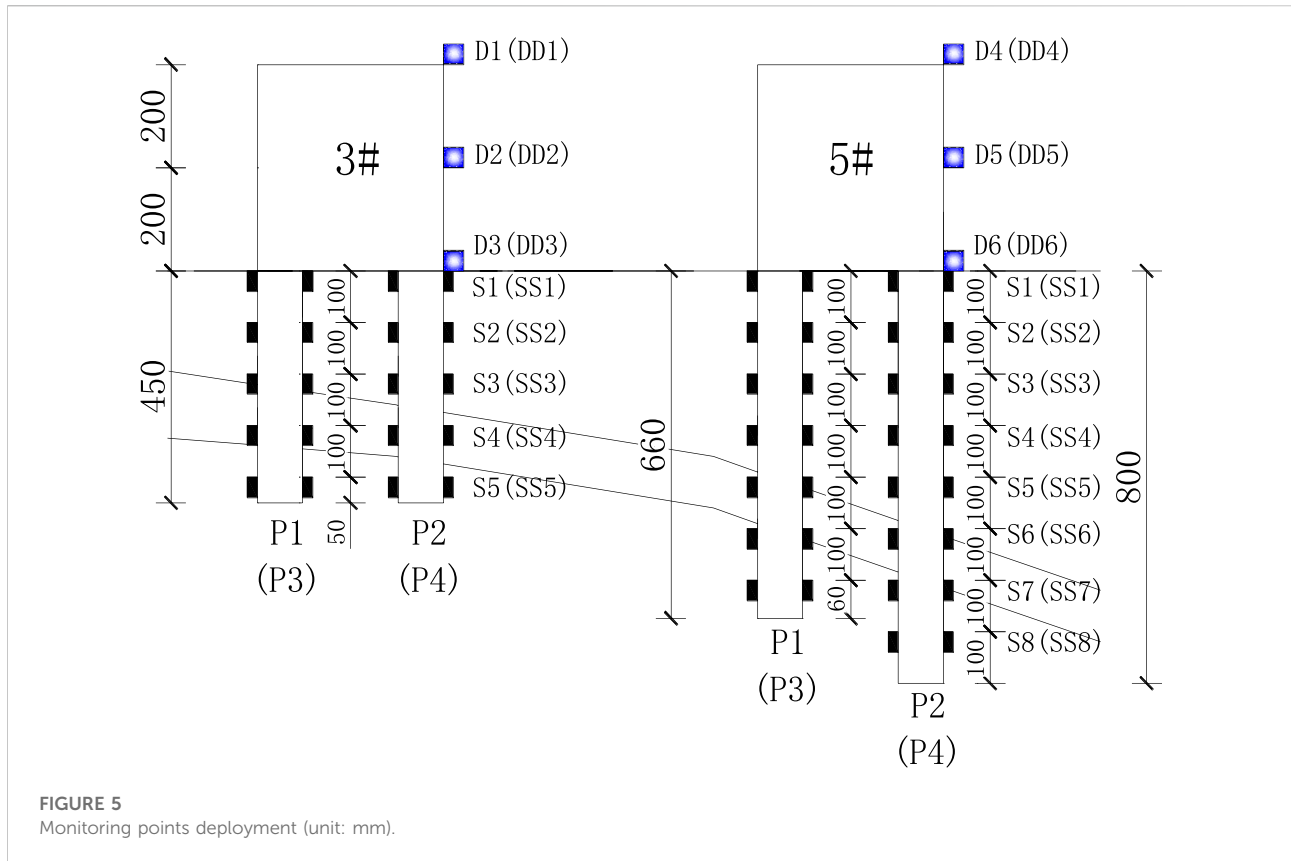


Rainfall added to the water content of the soil body, weakening the soil shear strength and affecting the dynamic response of the soil (White and Singham, 2012). By comparing the AAF distributions under different moisture contents, it can be seen that greater water content led to a stronger acceleration response of the bedrock, as presented in Figure 8 and Figure 9. This may be explained by the increase of bedrock unit weight as absorbing water. Also, container 3# in section I' showed a greater response under saturated moisture content, which suggests higher risks for the structure because of the existence of water in the tilted interlayer. Furthermore, piles that stick through the 3 soil layers improved the overall stability of the model by comparing it with the result of a simple slope (Cao et al., 2019).

Bending moment response of the piles

Bending moment history

Strain gauges attached to piles P1 - P4 of containers 3# and 5# at different depths were used to calendar the axial strain. The bending moment was converted through the method by Tokimatsu and Suzuki (2004). Figure 10 shows the bending moment history of measured points in P2 of container 5# with saturated water content under 0.15 g El Centro earthquake excitation. It can be seen that the bending moment near the soil interface increased, and reached the peak at the pile top, which means that the pile near the interface of soils and junction between the pile top and pile cap should have more attention paid to it.



Maximum bending moment

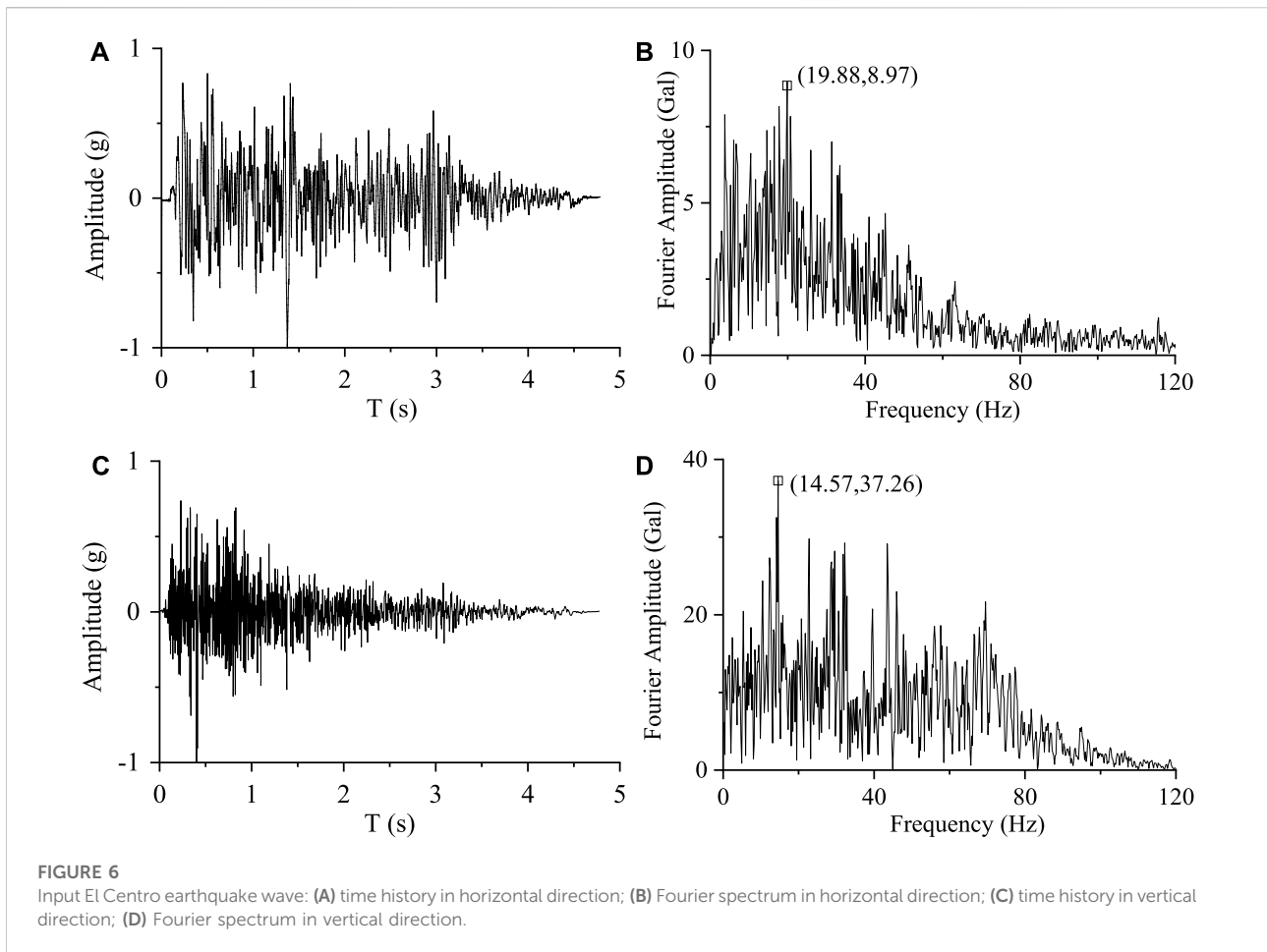
The bending moment responses of piles were investigated. Figure 11 shows the maximum bending moment of the piles beneath the disposal containers 3# and 5# with general moisture content. With respect to the piles of container 3#, it is shown that the maximum bending moment increased linearly with height and reached the maximum at the pile top. The possible reason is that the interlayer under container 3# was shallow and gentle, and it had a low moisture content. Plus, piles were inserted into the bedrock, which may possibly have led to the sliding of the covering layer. The bending moment mainly came from the inertial force of the container. In terms of container 5#, the influence of the interlayer was slight under small earthquakes, and the inertial force of the container was the major contributor to the bending moment. However, under stronger earthquakes, the bending moment rose because the sliding force at the interface of the soil layer increased. Tang and Ling (2014) also found that the bending moment of piles near the interface of two layers of soil increased. It is also shown that the bending moment of the pile at the upper part rose with the increase of the acceleration amplitude because the inertial force strengthened.

Figure 12 presents the peak bending moment distribution of the piles under disposal containers 3# and 5# under saturated moisture content. It is evident that the CC response was significantly influenced by the soil water content. With the decrease of

effective stress and shear strength caused by water, the bending moment of the piles near the interface of the soils under container 3# showed a rise. The bending moment of a pile's upper part was not as appreciable as the results shown for the same pile with general moisture content in Figure 11. Table 4 shows the maximum bending moment and the increase range with different moisture content. The increase range was "+" near the interface of the soils, while it reversed near the top piles. The possible reason is that the pile in the covering layer was thin, and shaking the container with the covering layer led to the main transformation of the pile at the interface of soils. For the piles under container 5#, similar results were found near the interface of soils due to the saturated moisture content. By comparing the bending moment distribution of piles under small earthquakes, it was seen that the saturated moisture content posed a great threat to the stability of the soil-pile-structure system. It was also shown that container 5#, which was located at the downhill, was more vulnerable than container 3# during an earthquake.

Displacement response of the disposal containers

In order to investigate the displacement response of the container under different earthquake amplitudes, laser displacement sensors



were used to record the displacement history. As the container near the downhill was more the concern, the maximum displacement distribution of disposal container 5# is shown in Figure 13. It is seen that the displacement response was almost linear. The peak displacement of the container rose along with the increase of the acceleration amplitude. The rotation angle of container 5# with general moisture content was not noticeable, with the value being about 0.05° . With saturated water content, the larger the acceleration amplitude, the greater the rotation angle of container #5. Also, it is seen that the displacements of measured points at the bottom of container 5# did not vary much under different moisture content, but there was a rise in the rotation angle during stronger earthquakes when the soil was highly moist, which suggests the water content in the interlayer influenced the rotation angel. When the soil was saturated, both translation and rotation were the motion modes of container 5#, while translation dominated when the moisture content was general. Table 5 shows the displacement value and of top container 5# with different moisture content. The increase range for saturated moisture content was "+", and it increased with increasing IAA. It means that the water should not be ignored under safety evaluation.

Discussion

Influence of interlayer soil

The elevation of the bedrock increased the AAF value, while it was not in the interlayer. At present, most of the research focuses on the dynamic response of pile foundation in homogeneous soil under earthquake action (Wilson, 1998; Miwa et al., 2006; He et al., 2009; Liu et al., 2022). The interface should not be ignored for slope stability and pile safety. Liu et al. (2015) also found the acceleration decreased in the interlayer through the shaking table test. Tang and Ling (2014) found that the bending moment reached a maximum level near the soil interface, and the piles were damaged when the sand soil was liquefied under 0.633 g earthquake excitation. Zhang et al. (2018) also found that the maximum bending moment appeared at the interface between loose sand and dense sand. But Huang et al. (2013) and Fan et al. (2016) found that the AAF of weak interlayer in bedding and counter-bedding slope was larger than those without a weak interlayer. The possible reason is related to the interlayer thickness, interlayer strength, wave reflection, and wave refraction (Yang et al.,

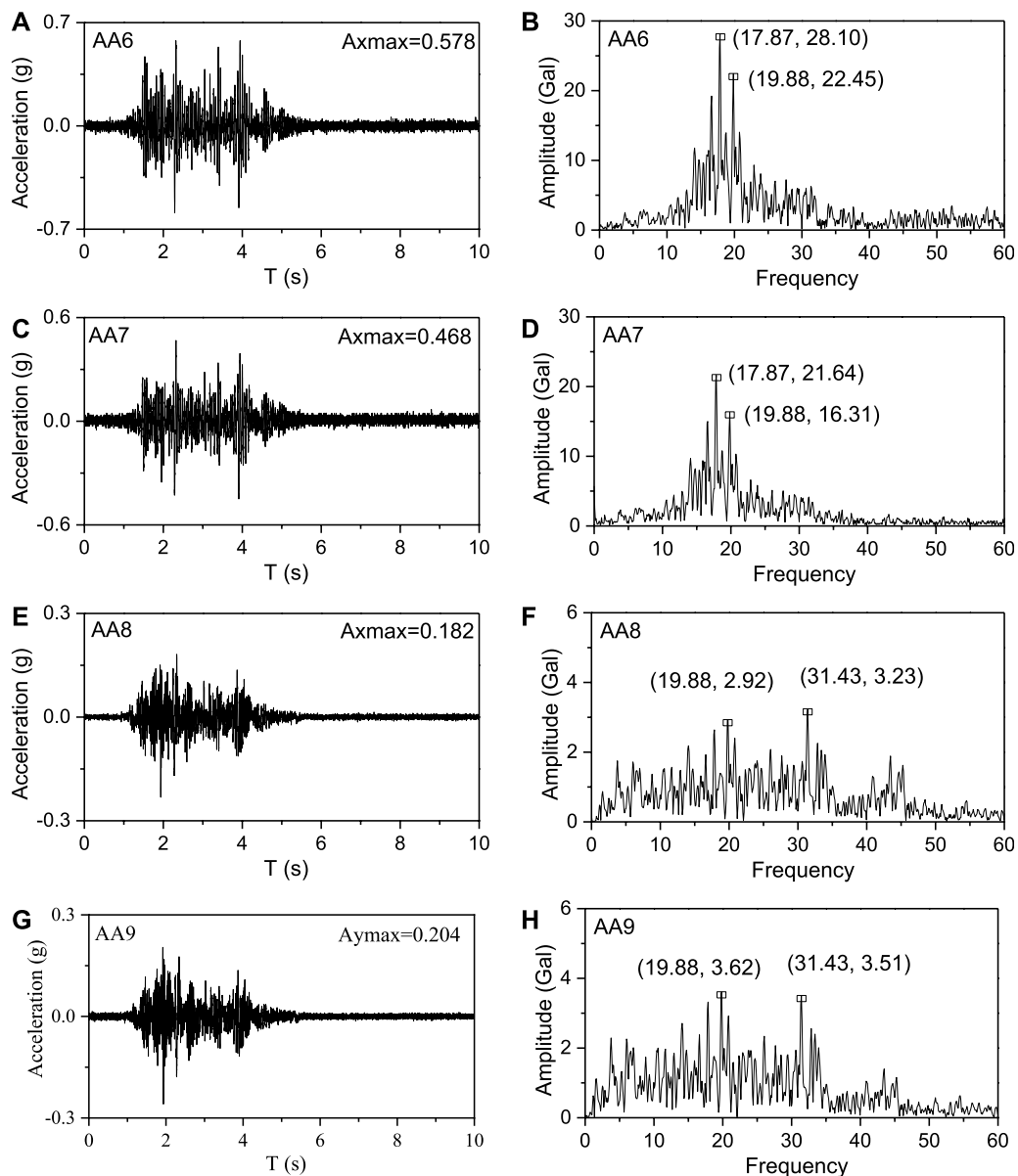


FIGURE 7

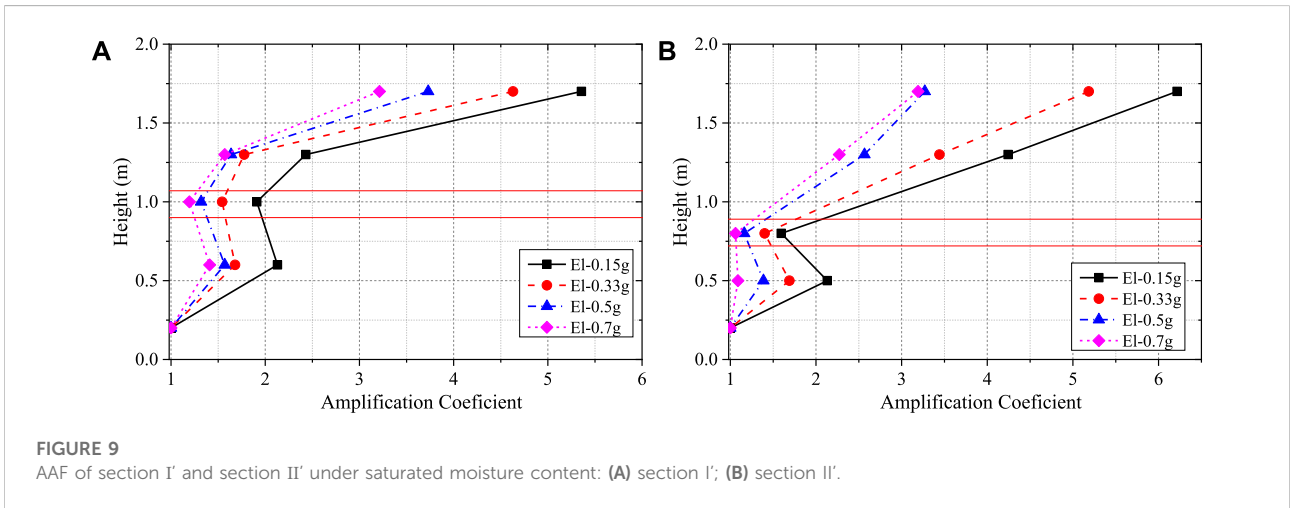
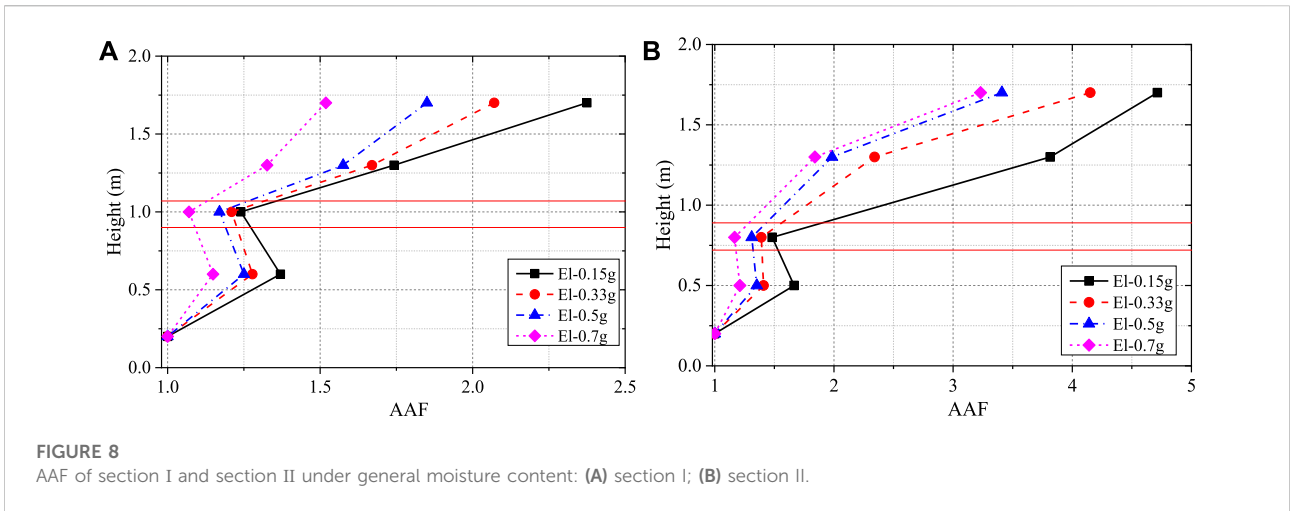
Acceleration time history and Fourier spectrum of measured points in section II' under 0.15 g earthquake excitation: (A) acceleration history of AA6 point; (B) Fourier spectrum of AA6 point; (C) acceleration history of AA7 point; (D) Fourier spectrum of AA7 point; (E) acceleration history of AA8 point; (F) Fourier spectrum of AA8 point; (G) acceleration history of AA9 point; (H) Fourier spectrum of AA9 point.

2012). The amplitude of dynamic response may be superimposed or weakened in the slope compared with homogenous slope.

Influence of rainfall

The results show that existence of water in the tilted interlayer resulted in a greater response of the container, and

there was infiltration effect for the weak interlayer. The rainfall splash erosion under different rainfall intensities was investigated by Majid and Sara (2016) and Sun et al. (2021). Lu et al. (2019) found that the structure stability was affected by uneven settlement caused by drying and wetting cycles of covering soil. There was an obvious creep characteristic for soft soil under high water content (Zhou et al., 2021). Liu et al. (2020) pointed out that the soil creep behavior was related to deformation, stress, strength, and time. The slope stability



decreased with the rainfall time increasing, and the area with greatest sliding risk was slope foot (Yao et al., 2021). Also, the unit soil mass weight increased, and the effect stress decreased during rainfall (Terzaghi 1950; White and Singham, 2012). The above soil features during rainfall decreased the structure stability obviously. Although the influence of rainfall was significant, the critical rainfall threshold is not discussed in this article, and it will be studied in the future.

Limitations of physical test

The observed results are typical site seismic response with reinforcement under earthquake and rainfall. It should be noted that the seismic response of system was related to the seismic input motions, reinforcement type, and rainfall simulation.

1) El Centro waves with different amplitude were chosen as excitation, and other earthquake waves with different frequency spectrum were neglected in the presented tests. More model tests should be conducted if different earthquake spectrum is considered, and it will be studied in the future. 2) The prototype piles were in a group, and 4 model piles were deployed at the corners of the container based on the total flexural rigidity similarity of piles in consideration of scale limitation. 3) The rainfall simulation could be process simulation or end simulation. The water content of soil was set based on rainfall end simulation. The coupling condition could reappear in this test.

Therefore, the results of this study could be used to assess seismic response with reinforcement under earthquake and rainfall, considering the limitation of the model test.

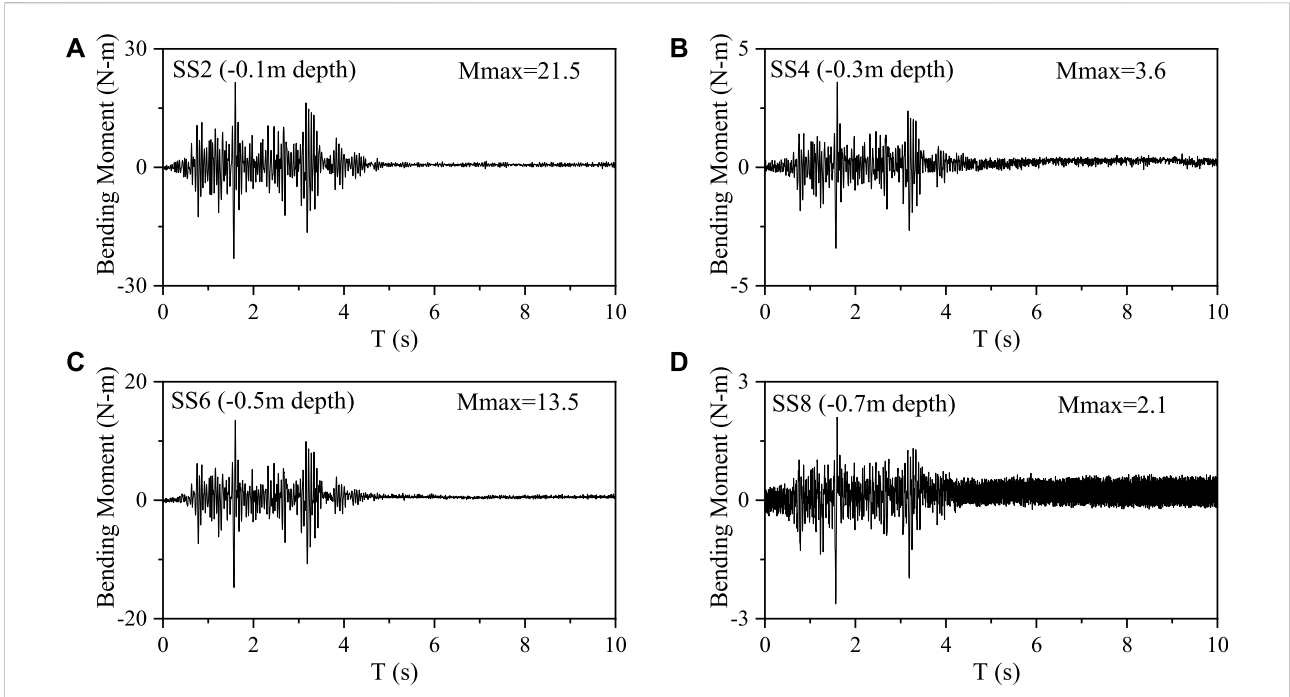


FIGURE 10
 Bending moment history of measured points in P2 of container 5# with saturated moisture content under 0.15 g earthquake excitation: (A) SS2 point; (B) SS4 point; (C) SS6 point; (D) SS8 point.

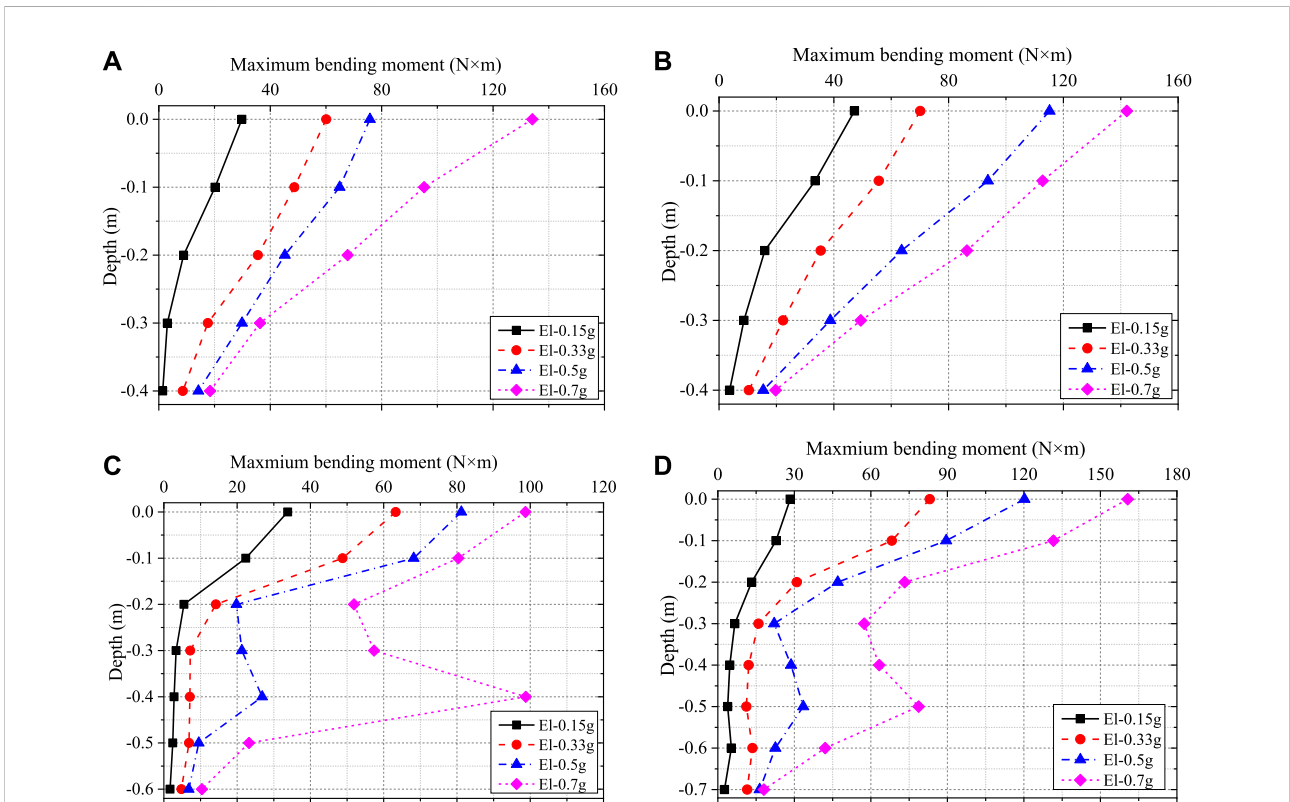


FIGURE 11
 Peak bending moment of the piles beneath disposal containers: (A) 3#-P1; (B) 3#-P2; (C) 5#-P1; (D) 5#-P2 with general moisture content.

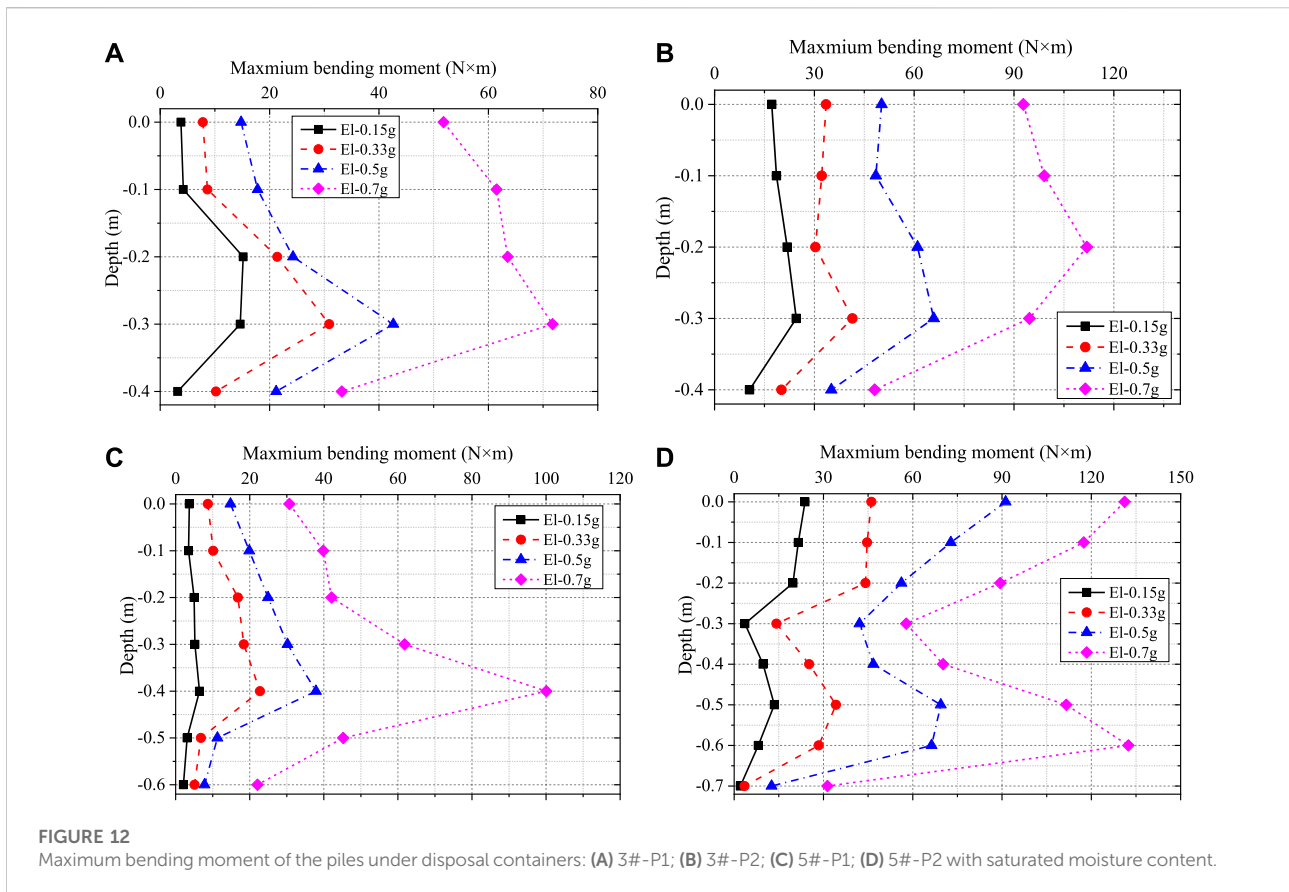


TABLE 4 Maximum bending moment and increase range with different moisture content.

Location		IAA=0.15 g			IAA=0.5 g		
		MBM (N·m)		IR (%)	MBM (N·m)		IR (%)
		MC-1	MC-2		MC-1	MC-2	
3#	P1(0 m)	29.8	3.8	-87.25	75.8	14.8	-80.47
3#	P2(0 m)	47.2	17.2	-63.56	115.2	50.2	-56.42
5#	P1(0 m)	33.8	3.7	-89.05	81.2	14.8	-81.77
5#	P2(0 m)	28.4	23.8	-16.20	120.2	91.2	-24.13
3#	P1(-0.3 m)	3.0	14.6	386.67	29.9	42.6	42.47
3#	P2(-0.3 m)	8.7	24.5	181.61	38.8	65.9	69.85
5#	P1(-0.4 m)	3.3	6.4	93.94	26.8	37.9	41.42
5#	P2(-0.4 m)	4.7	9.7	106.38	28.7	46.7	62.72

Notes: IAA, input acceleration amplitude; MBM, maximum bending moment; MC-1, general moisture content; MC-2, saturated moisture content; IR, increase range.

Conclusion

The test model in this study is a prototype of a sandstone site in China. The test was conducted to research the seismic

response of structures in multi-tilted-layered soils under earthquake and rainfall. The acceleration distribution, bending moment of piles, and displacement response of the container were analyzed. Some conclusions can be drawn as follows:

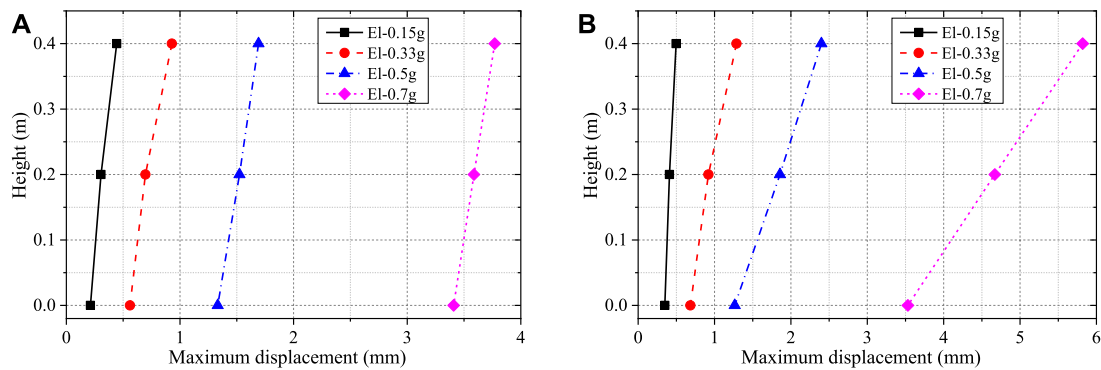


FIGURE 13 Maximum displacement distribution of disposal container 5# with different moisture content: (A) low moisture content; (B) high moisture content.

TABLE 5 Displacement of top container 5# and increase range with different moisture content.

IAA(g)	DTC(mm)		IR(%)	RA(°)		IR (%)
	MC-1	MC-2		MC-1	MC-2	
0.15	0.443	0.497	12.14	0.023	0.028	21.98
0.33	0.929	1.287	38.56	0.053	0.086	63.40
0.5	1.692	2.399	41.78	0.052	0.162	215.23
0.7	3.770	5.820	54.36	0.052	0.328	533.27

Notes: IAA, input acceleration amplitude; DTC, displacement of top container; IR, increase range; MC-1, general moisture content; MC-2, saturated moisture content; RA, rotation angle.

- 1) The elevation of the bedrock increased the AAF value, while it was not in the interlayer. The existence of water in the tilted interlayer resulted in a greater response of the container, and there was an infiltration effect for the weak interlayer. Also, the acceleration response was weakened when the earthquake amplitude increased.
- 2) The inertial force of the container and potential sliding force of the covering layer played major roles in making the maximum bending moment at the pile. The existence of water promoted the increase of bending moment of piles, which added to the potential risk of system instability.
- 3) The motion mode of the container with general moisture content was translation, and the rotation angle of the container with saturated moisture content increased with the rise of the earthquake amplitude. Higher water content led to larger displacement of the container.

- 4) The tilted weathered layer and different moisture content should be considered during earthquakes by analyzing the acceleration, Fourier Spectrum, and bending moment. Proper reinforcement should be considered in the tilted interface for this typical site.

Data availability statement

The original contributions presented in the study are included in the article/Supplementary material, and further inquiries can be directed to the corresponding author.

Author contributions

JZ designed the research. LC performed the shaking table tests, and HS contributed to the data analysis. JZ, LC, and HS contributed to the writing.

Conflict of interest

The authors declare that the research was conducted in the absence of any commercial or financial relationships that could be construed as a potential conflict of interest.

Publisher's note

All claims expressed in this article are solely those of the authors and do not necessarily represent those of their affiliated organizations, or those of the publisher, the editors, and the reviewers. Any product that may be evaluated in this article, or claim that may be made by its manufacturer, is not guaranteed or endorsed by the publisher.

References

- Adler, R. F. (2008). Predicting global landslide spatiotemporal distribution: Integrating landslide susceptibility zoning techniques and real-time satellite rainfall estimates. *Int. J. Sediment Res.* 23 (3), 249–257. doi:10.1016/s1001-6279(08)60022-0
- Badry, P., and Satyam, N. (2017). Seismic soil structure interaction analysis for asymmetrical buildings supported on piled raft for the 2015 Nepal earthquake. *J. Asian Earth Sci.* 133, 102–113. doi:10.1016/j.jseas.2016.03.014
- Bhattacharya, S., Lombardi, D., Dihoru, L., Dietz, M. S., Crewe, A. J., and Taylor, C. A. (2012). Model container design for soil-structure interaction studies. *Role Seismic Test. Facil. Performance-Based Earthq. Eng.* 22, 135–158. doi:10.1007/978-94-007-1977-4_8
- Brand, L. (1957). The Pi theorem of dimensional analysis. *Arch. Ration. Mech. Anal.* 1 (1), 35–45. doi:10.1007/BF00297994
- Brandenberg, S. J., Boulanger, R. W., Kutter, B. L., and Chang, D. (2005). Behavior of pile foundations in laterally spreading ground during centrifuge tests. *J. Geotech. Geoenviron. Eng.* 131131 (11), 137811–141391. doi:10.1061/(asce)1090-0241(2005)131:11(1378)
- Cao, L., Fu, X., Wang, Z., Zhou, Y., Liu, F., and Zhang, J. (2018). Seismic responses of the steel-strip reinforced soil retaining wall with full-height rigid facing from shaking table test. *J. Mt. Sci.* 15 (5), 1137–1152. doi:10.1007/s11629-017-4598-2
- Cao, L., Zhang, J., Wang, Z., Liu, F., Liu, Y., and Zhou, Y. (2019). Dynamic response and dynamic failure mode of the slope subjected to earthquake and rainfall. *Landslides* 16 (8), 1467–1482. doi:10.1007/s10346-019-01179-7
- Chang, B. J., and Hutchinson, T. C. (2013). Experimental investigation of plastic demands in piles embedded in multi-layered liquefiable soils. *Soil Dyn. Earthq. Eng.* 49, 146–156. doi:10.1016/j.soildyn.2013.01.012
- Choobasthi, A. J., Saadati, M., and Tavakoli, H. R. (2012). Seismic response of pile foundations in liquefiable soil: Parametric study. *Arab. J. Geosci.* 5 (6), 1307–1315. doi:10.1007/s12517-011-0291-x
- Ciurleo, M., Mandaglio, M. C., and Moraci, N. (2018). Landslide susceptibility assessment by trigers in a frequently affected shallow instability area. *Landslides* 16 (4), 175–188. doi:10.1007/s10346-018-1072-3
- Curtis, W. D., Logan, J. D., and Parker, W. A. (1982). Dimensional analysis and the pi theorem. *Linear Algebra its Appl.* 47, 117–126. doi:10.1016/0024-3795(82)90229-4
- Elgamal, A., Yan, L., Yang, Z., and Conte, J. P. (2008). Three-dimensional seismic response of Humboldt Bay bridge-foundation-ground system. *J. Struct. Eng. (N. Y. N. Y.)* 134134 (7), 11657–21176. doi:10.1061/(asce)0733-9445(2008)134:7(1165)
- Fan, G., Zhang, J., Wu, J., and Yan, K. (2016). Dynamic response and dynamic failure mode of a weak intercalated rock slope using a shaking table. *Rock Mech. Rock Eng.* 49 (8), 3243–3256. doi:10.1007/s00603-016-0971-7
- GB/T 17742-2008 (2008). *The Chinese seismic intensity scale*. Beijing: China Standard Press.
- Guo, Z., Shi, Y., Huang, F., Fan, X., and Huang, J. (2021). *Landslide susceptibility zonation method based on c5.0 decision tree and k-means cluster algorithms to improve the efficiency of risk management*.
- He, L., Elgamal, A., Abdoun, T., Abe, A., Dobry, R., Hamada, M., et al. (2009). Liquefaction-induced lateral load on pile in a medium Dr sand layer. *J. Earthq. Eng.* 13 (7), 916–938. doi:10.1080/13632460903038607
- Huang, F., Chen, J., Liu, W., Huang, J., Hong, H., and Chen, W. (2022b). Regional rainfall-induced landslide hazard warning based on landslide susceptibility mapping and a critical rainfall threshold. *Geomorphology* 408, 108236. doi:10.1016/j.geomorph.2022.108236
- Huang, F., Tao, S., Chang, Z., Huang, J., Jiang, S., Zhu, L., et al. (2021). Efficient and automatic extraction of slope units based on multi-scale segmentation method for landslide assessments. *Landslides* 18 (11), 3715–3731. doi:10.1007/s10346-021-01756-9
- Huang, F., Yan, J., Fan, X., Yao, C., Huang, J., Chen, W., et al. (2022a). Uncertainty pattern in landslide susceptibility prediction modelling: effects of different landslide boundaries and spatial shape expressions. *Geosci. Front.* 13 (2), 101317. doi:10.1016/j.gsf.2021.101317
- Huang, R., Zhao, J., Ju, N., Li, G., Lee, M. L., and Li, Y. (2013). Analysis of an anti-dip landslide triggered by the 2008 wenchuan earthquake in China. *Nat. Hazards (Dordr.)* 68 (2), 1021–1039. doi:10.1007/s11069-013-0671-5
- Jiang, S. H., and Huang, J. S. (2016). Efficient slope reliability analysis at low-probability levels in spatially variable soils. *Comput. Geotech.* 75, 18–27. doi:10.1016/j.compgeo.2016.01.016
- Liu, F., Li, Z., Jiang, M., Frattini, P., and Crosta, G. (2016). Quantitative liquefaction-induced lateral spread hazard mapping. *Eng. Geol.* 207, 36–47. doi:10.1016/j.enggeo.2016.04.001
- Liu, H., Xu, Q., and Zhou, F. (2015). Shaking table test for seismic responses of slopes with a weak interlayer. *Chin. J. Rock Mech. Eng.* 5, 994–1005. doi:10.13722/j.cnki.jrme.2014.0903
- Liu, J., Jing, H., Meng, B., Wang, L., Yang, J., and Zhang, X. (2020). A four-element fractional creep model of weakly cemented soft rock. *Bull. Eng. Geol. Environ.* 79 (10), 5569–5584. doi:10.1007/s10064-020-01869-w
- Liu, Q., Zhuang, H., Wu, Q., Zhao, K., and Chen, G. (2022). Experimental study on dynamic modulus and damping ratio of rubber-sand mixtures over a wide strain range. *J. Earthq. Tsunami* 16 (02). doi:10.1142/S1793431121400066
- Lu, Y., Liu, S., Alonso, E., Wang, L., Xu, L., and Li, Z. (2019). Volume changes and mechanical degradation of a compacted expansive soil under freeze-thaw cycles. *Cold Regions Sci. Technol.* 157, 206–214. doi:10.1016/j.coldregions.2018.10.008
- Maiorano, R. M. S., de Sanctis, L., Aversa, S., and Mandolini, A. (2009). Kinematic response analysis of piled foundations under seismic excitation. *Can. Geotech. J.* 46 (5), 571–584. doi:10.1139/T09-004
- Majid, M., and Sara, A. S. (2016). Effects of rain intensity, slope gradient and particle size distribution on the relative contributions of splash and wash loads to rain-induced erosion. *Geomorphology*. 253, 159–167. doi:10.1016/j.geomorph.2015.10.010
- Martin, G. R., and Chen, C. Y. (2005). Response of piles due to lateral slope movement. *Comput. Struct.* 83 (8-9), 588–598. doi:10.1016/j.compstruc.2004.11.006
- Mashhoud, H. J., Yin, J. H., Panah, A. K., and Leung, Y. F. (2018). Shaking table test study on dynamic behavior of micropiles in loose sand. *Soil Dyn. Earthq. Eng.* 110, 53–69. doi:10.1016/j.soildyn.2018.03.008
- Meymand, P. J. (1998). *Shaking table scale model tests of nonlinear soil-pile-superstructure interaction in soft clay*. Doctoral dissertation. Berkeley: University of California.
- Michel, G., Kobiyama, M., and Goerl, R. (2014). Comparative analysis of shalstab and sinmap for landslide susceptibility mapping in the cunha river basin, southern Brazil. *J. Soils Sediments* 14 (7), 1266–1277. doi:10.1007/s11368-014-0886-4
- Miwa, S., Ikeda, T., and Sato, T. (2006). Damage process of pile foundation in liquefied ground during strong ground motion. *Soil Dyn. Earthq. Eng.* 26 (2-4), 325–336. doi:10.1016/j.soildyn.2005.05.001
- Samuele, S., Veronica, T., Ascanio, R., Filippo, C., and Nicola, C. (2018). Combination of rainfall thresholds and susceptibility maps for dynamic landslide hazard assessment at regional scale. *Front. Earth Sci. (Lausanne)*. 6, 85. doi:10.3389/feart.2018.00085
- Segoni, S., Piciullo, L., and Gariano, S. L. (2018). A review of the recent literature on rainfall thresholds for landslide occurrence. *Landslides*. 15, 1483–1501. doi:10.1007/s10346-018-0966-4
- Sun, S., Zhang, Y., and Lei, P. (2021). Mass exchange of water and soil on the soil surface in the rainfall splash erosion. *Front. Earth Sci. (Lausanne)*. 9, 1015. doi:10.3389/feart.2021.739804
- Tang, C., Qi, X., Ding, J., Yang, T. P., and Luo, Z. F. (2010). Dynamic analysis on rainfall-induced landslide activity in high seismic intensity areas of the Wenchuan earthquake using remote sensing image. *Earth Science/Diqiu Kexue* 35 (2).
- Tang, L., and Ling, X. (2014). Response of a RC pile group in liquefiable soil: A shake-table investigation. *Soil Dyn. Earthq. Eng.* 67, 301–315. doi:10.1016/j.soildyn.2014.10.015
- Terzaghi, K. (1950). Mechanism of landslides. Application of geology to engineering practice. *Geol. Soc. Am.*, 83–123.
- Tokimatsu, K., and Suzuki, H. (2004). Pore water pressure response around pile and its effects on py behavior during soil liquefaction. *Soils Found.* 44 (6), 101–110. doi:10.3208/sandf.44.6_101
- Tokimatsu, K., Suzuki, H., and Sato, M. (2005). Effects of inertial and kinematic interaction on seismic behavior of pile with embedded foundation. *Soil Dyn. Earthq. Eng.* 25 (7-10), 753–762. doi:10.1016/j.soildyn.2004.11.018
- Uzuoka, R., Sento, N., Kazama, M., Zhang, F., Yashima, A., and Oka, F. (2007). Three-dimensional numerical simulation of earthquake damage to group-piles in a liquefied ground. *Soil Dyn. Earthq. Eng.* 27 (5), 395–413. doi:10.1016/j.soildyn.2006.10.003

Wang, Z., Fan, G., Han, J., Liao, W., and Zhang, J. (2013). *Reference strain γ_r in hyperbolic modeling of dynamic shear modulus of soils*, 271–278. IACGE 2013: Challenges and Recent Advances in Geotechnical and Seismic Research and Practices.

White, J. A., and Singham, D. I. (2012). Slope stability assessment using stochastic rainfall simulation. *Procedia Comput. Sci.* 9, 699–706. doi:10.1016/j.procs.2012.04.075

Wilson, D. W. (1998). *Soil-pile-superstructure interaction in liquefying sand and soft clay*. Doctoral dissertation. Davis: University of California.

Yang, G., Wu, F., Dong, J., and Qi, S. (2012). Study of dynamic response characters and failure mechanism of rock slope under earthquake. *Chin. J. Rock Mech. Eng.* 31 (4), 696–702. (in Chinese). doi:10.3969/j.issn.1000-6915.2012.04.007

Yao, Y., Li, J., Xiao, Z., and Xiao, H. (2021). Soil-water characteristics and creep deformation of unsaturated expansive subgrade soil: Experimental test and simulation. *Front. Earth Sci. (Lausanne)*. 9, 1141. doi:10.3389/feart.2021.783273

Zhang, X., Tang, L., Ling, X., Chan, A. H. C., and Lu, J. (2018). Using peak ground velocity to characterize the response of soil-pile system in liquefying ground. *Eng. Geol.* 240, 62–73. doi:10.1016/j.enggeo.2018.04.011

Zhou, F., Wang, L., and Liu, H. (2021). A fractional elasto-viscoplastic model for describing creep behavior of soft soil. *Acta Geotech.* 16 (1), 67–76. doi:10.1007/s11440-020-01008-5